Journal of Marine Systems 257 (2026) 104261

Contents lists available at ScienceDirect

Journal of Marine Systems

journal homepage: www.elsevier.com/locate/jmarsys

Coupled biogeochemical, biological, and physical controls on nitrogen fixation during a cyanobacterial bloom in the Baltic Sea

Sören Iwe [a,*], Bernd Schneider [a], Lumi Haraguchi [b], Kaisa Kraft [b], Gregor Rehder [a], Jukka Seppälä [b], Ulf Gräwe [a], Carsten Mönnig [c], Oliver Schmale [a]

[a] Leibniz Institute for Baltic Sea Research Warnemünde (IOW), Seestraße 15, 18119 Rostock, Germany
[b] Finnish Environment Institute (Syke), Latokartanonkaari 11, 00790 Helsinki, Finland
[c] German Aerospace Center (DLR), Earth Observation Center, Kalkhorstweg 53, 17235, Neustrelitz, Germany

ARTICLE INFO

Dataset link: Coupled Biogeochemical, Biological, and Physical Controls on Nitrogen Fixation during a Cyanobacterial Bloom in the Baltic Sea (Original data)

Keywords:
Baltic Sea
Cyanobacteria
N_2 fixation
GE-MIMS
Carbon dioxide

ABSTRACT

Summer filamentous cyanobacterial blooms strongly influence the biogeochemistry of the Baltic Sea. In surface water, they sustain organic matter (OM) production via N_2 fixation despite the depletion of dissolved inorganic nitrogen (DIN). In deeper water, remineralization of this OM contributes to O_2 depletion and H_2S formation, thereby promoting Baltic Sea hypoxia/anoxia. Primary production by cyanobacteria also drives a characteristic summer drawdown of total dissolved CO_2 (C_T). While this biogeochemical signal is thought to reflect N_2 fixation, direct observational evidence supporting this link remains limited. In addition, key questions remain regarding the factors regulating bloom initiation and intensity.

This study applied a multi-method approach, combining continuous high-resolution surface water measurements of biogeochemical and biological variables made from the ship of opportunity *Finnmaid* traveling between Travemünde (Germany) and Helsinki (Finland), with modeled physical parameters, to investigate a cyanobacterial hotspot identified in summer 2023. During the 2.5-week C_T drawdown (~1500 to ~1325 µmol/kg) in June, at the entrance to the Gulf of Finland, 70% of the decrease occurred in the final five days and coincided with a sharp increase in filamentous cyanobacterial biomass and pronounced N_2 undersaturation. Our observations indicate that once the cyanobacterial biomass has been accumulated during favorable environmental conditions, their impacts can be drastic to the carbon system. Our results link N_2 fixation with the C_T decline in surface water, while also demonstrating that ecosystem productivity is enhanced by co-occurring phytoplankton species, which likely benefit from the nitrogen released by cyanobacterial N_2 fixation.

1. Introduction

Biogeochemical studies linking chemical signals to biological processes and the organisms that drive them can provide essential insights into ecosystem functioning in the marine environment (Salihoglu et al., 2013; York, 2018). Concentrations of dissolved gases are especially informative, as they reflect both biologically driven activities, such as those contributing to carbon cycling and shaping oxygen dynamics, and physical phenomena, including mixing events within the water column. In this context, continuous measurement of the partial pressure of CO_2 (pCO_2) in surface water is a powerful tool for characterizing the seasonal progression of biological production in aquatic systems (Thomas and Schneider, 1999; Schneider et al., 2015; Schneider and Müller, 2018).

In the Baltic Sea, such measurements have been conducted since 2003 (Schneider and Müller, 2018) using a fully automated system installed on a ship of opportunity (SOOP), initially the MS *Finnpartner* (2003–2006) and later the MS *Finnmaid* (2006–present). This platform traverses across the Baltic Proper, covering more than 1000 km, four to five times per week, thereby obtaining spatially extensive and temporally highly resolved data throughout the year.

From those measurements consistent seasonal patterns of two biological production events are apparent. The first production event is the spring bloom, which is fueled by the available nitrate in surface waters and typically exhausts this pool as it progresses. The second occurs in summer and is dominated by filamentous cyanobacteria, which overcome the post-spring depletion of nitrate by converting the dissolved molecular nitrogen in surface waters into bioavailable compounds (N_2 fixation, Stal et al., 2003; Schneider et al., 2014a). By sustaining biomass

* Corresponding author.
E-mail address: soeren-iwe@web.de (S. Iwe).

https://doi.org/10.1016/j.jmarsys.2026.104261
Received 16 April 2026; Received in revised form 24 April 2026; Accepted 13 July 2026
Available online 15 July 2026
0924-7963/© 2026 The Authors. Published by Elsevier B.V. This is an open access article under the CC BY license (http://creativecommons.org/licenses/by/4.0/).

production even in the absence of dissolved inorganic nitrogen (DIN) in surface waters, these extensive cyanobacterial blooms amplify the symptoms of eutrophication in the Baltic Sea and are thus of major concern for the Baltic Sea health status (Vahtera et al., 2007). Furthermore, several dominant cyanobacterial species produce toxins that may adversely affect ecosystem biodiversity (Karjalainen et al., 2007).

Depending on the physical, meteorological, and biogeochemical conditions of the respective years and on the methodological approaches, estimates of nitrogen input via N_2 fixation in the central Baltic Sea range between 310 and 792 kt/year (Rolff et al., 2007). As these amounts are of the same order of magnitude as the combined nitrogen inputs from riverine discharge and atmospheric deposition (HELCOM, 2021a), N_2 fixation clearly plays a key role in the nitrogen budget of the Baltic Sea.

Regular assessments of the nitrogen budget of the Baltic Sea, including the contribution of N_2 fixation, are essential to obtain an accurate picture of the ecological status of the Baltic Sea and its development, especially due to climate change induced shifts in the environmental conditions such as rising sea surface temperatures (SSTs) and intensified stratification (O'Neil et al., 2012; Liblik and Lips, 2019). The approaches developed to quantify N_2 fixation include those based on the analysis of discrete water samples, such as the ^{15}N incubation method (Montoya et al., 1996). However, due to the patchy distribution of cyanobacterial blooms, substantial uncertainties can arise when data from sparse discrete samplings are spatially and temporally interpolated or extrapolated. Furthermore, these methods are labor-intensive and time consuming, which limits their applicability to extended spatio-temporal scales. This limitation can be avoided by using pCO_2 data collected from a SOOP to derive the total CO_2 (C_T; synonymous with dissolved inorganic carbon, DIC) concentration and thereby estimate net community production (NCP). The magnitude of N_2 fixation can then be estimated indirectly, based on the mean C/N ratio of particulate organic matter (POM). This approach (Schneider et al., 2014a) relies on the assumption that summer biomass production occurs in the absence of DIN and that nitrogen must therefore be supplied through N_2 fixation. We evaluated the validity of this assumption using additional continuous biogeochemical and biological measurements performed on the SOOP platform, including determinations of phytoplankton biomass, community composition, and gas dynamics related to biomass production and N_2 fixation. Accordingly, the objectives of our study were:

(1) To use pCO_2 records to identify a N_2 fixation hotspot along the track of SOOP Finnmaid;
(2) To place the N_2 fixation hotspot within the seasonal context of biological production;
(3) To characterize the intensity of N_2 fixation at the hotspot using biogeochemical and biological approaches;
(4) To describe the progression of a cyanobacterial bloom and investigate the interactions between related physical, biogeochemical, and biological processes.

2. Materials and methods

2.1. Study area and sampling platform

Throughout 2023, physical, biogeochemical, and biological parameters of surface waters were measured on board the SOOP *Finnmaid*. Concentrations of dissolved N_2, O_2, and Ar were determined (Section 2.2.4) during a 5-week period in summer (June 15–July 19), when the likelihood of capturing a cyanobacterial bloom in the Baltic Sea was high (e.g., Wasmund, 1997). The SOOP commutes between the western Gulf of Finland (Helsinki) and Mecklenburg Bight (Travemünde) with a 3 day roundtrip time interval, capturing the main regional variation across the Baltic Proper along the way (Fig. 1). The route leads either east or west of Gotland. Based on a strong production signal in the pCO_2 data (Section 3.1) and satellite imagery confirming the high abundance of cyanobacteria, a region at the entrance to the Gulf of Finland (EGF; ~22.0–24.5°E) with an extension of ~150 km along the track was selected as the main study area (Fig. 1). This location is characterized by its proximity to land and the strong influence of riverine inputs.

Following the ship's schedule, the EGF region was sampled, on average, at around 02:30 UTC (05:30 local time) during the *Finnmaid*'s arrival in the Gulf and around 16:00 UTC (19:00 local time) on its return leg from Helsinki. The short time interval between these two sampling

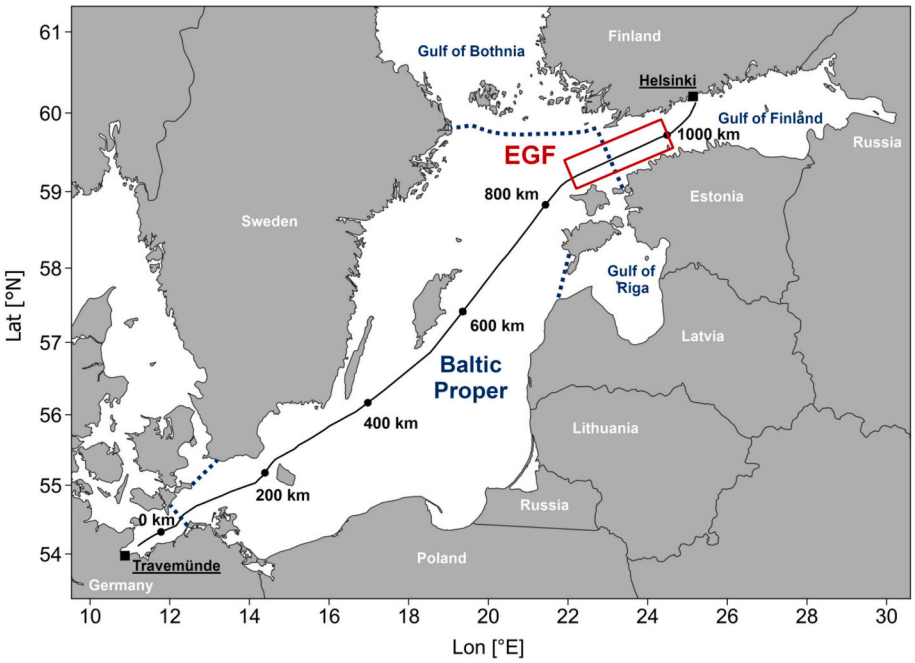


Fig. 1. The eastern transect (black line) based on the route of the SOOP *Finnmaid* between Helsinki (Finland) and Travemünde (Germany). The area corresponding to the entrance to the Gulf of Finland (EGF), indicated by the red box, was investigated in detail in this study. The dashed lines indicate the boundaries of the Baltic Proper according to HELCOM (2021b). (For interpretation of the references to colour in this figure legend, the reader is referred to the web version of this article.)

events was 13.5 h, while the long interval, from the return measurement until the next entry into the EGF, was approximately 58.5 h, reflecting the time required for the vessel to complete the round trip to Travemünde and back. The duration of observations in the main observation area of this study on each transect was approximately 4 h. The ship's water inlet is at ~5 m depth, depending on the vessel's loading condition. The surface water is pumped with a pressure of 1 bar and distributed to different measurement systems (Section 2.2).

2.2. Instrumentation and measurements

This study was a collaboration between the Leibniz Institute for Baltic Sea Research (IOW) and the Finnish Environment Institute (Syke). The instruments (Gülzow et al., 2013) operated by the IOW on the SOOP measure dissolved gas concentrations (Sections 2.2.1 and 2.2.2) as part of the European Integrated Carbon Observation System Research Infrastructure (ICOS RI). A FerryBox system records continuously fluorescence, (see the detailed description in Kaitala et al., 2008), SST and salinity (SBE 45, Sea-Bird Electronics, USA) and other environmental parameters, while the position of the SOOP *Finnmaid* is recorded using GPS. The system also includes an automated water sampler for determinations of nutrients and chlorophyll *a* (Chl *a*) concentrations. In 2023, the observational setup included an Imaging FlowCytobot (IFCB) to characterize the phytoplankton community.

2.2.1. pCO_2 measurements

Continuous pCO_2 measurements, used in this study to identify and quantify production events, were obtained following well-established methods (e.g., Gülzow et al., 2011; Schneider et al., 2014a, 2014b), using a combined bubble/shower-type equilibrator system coupled with the infrared detection of CO_2 (MCA, Los Gatos Research) in equilibrated air. As the cited publications provide a comprehensive description of the methodology, only the most important aspects are described here.

The measured mole fraction of CO_2 (xCO_2) is corrected to that in dry air using the mole fraction H_2O (xH_2O) data from the same analyzer. It is then converted to pCO_2 according to the atmospheric pressure and the water vapor saturation in the equilibrator (Weiss and Price, 1980). The system is calibrated using a set of three calibration gases with an xCO_2 of ~200, 400, and 800 ppm, which are obtained from the Central Analytical Lab of ICOS in Jena. Calibration gas CO_2 mole fractions have an accuracy better than 0.2 ppm. The equilibration time (τ) is <4 min at a water flow rate of 10 L/min. For a mean vessel speed of 20 knots, this results in a spatial resolution of <10 km. The data are bin-averaged at 1-min intervals.

2.2.2. GE-MIMS for N_2, Ar and O_2 measurements

N_2 fixation and O_2 production were qualitatively assessed by measuring the concentrations of dissolved gases (N_2, Ar, and O_2) using a Gas-Equilibrium Membrane-Inlet Mass Spectrometer (GE-MIMS) specifically designed for long-term observations on a SOOP, as described in Iwe et al. (2025).

The GE-MIMS's membrane equilibrator (Liquicel MM series 1.8 × 8.75, model G541) facilitates the equilibration of dissolved atmospheric gases in seawater with a gas phase. Continuous measurements of the mole fractions of N_2, Ar, and O_2 in the gas phase by mass spectrometry enable the calculation of their concentrations based on the total pressure and the corresponding solubility constants, obtained from Hamme and Emerson (2004) for N_2 and Ar and from Weiss (1970) for O_2. Calibration is performed automatically once per hour using a standard gas with a composition similar to that of the atmosphere, ensuring an accuracy of 1.1 µmol/L for N_2, 0.005 µmol/L for Ar, and 0.6 µmol/L for O_2. Given a water flow rate of 2 L/min through the membrane, equilibration times of 4.8 min for N_2, 3 min for Ar, and 3.2 min for O_2 are achieved. At an average ship speed of 20 knots, this results in a spatial resolution of ~12 km for N_2. The concentrations of the respective gases are bin-averaged at 1-min intervals.

2.2.3. Phytoplankton community measurements

The phytoplankton community was quantified continuously (~ every 23 min) using an IFCB (McLane; Olson and Sosik, 2007), with a Chl *a* trigger (excitation/emission: 636/680 nm) set to target only autofluorescent cells, thereby largely excluding non-living particles. The dynamic size range of IFCB is 5–150 µm, thus it does not record the picophytoplankton and the smallest nanophytoplankton. However, cyanobacteria filaments up to 300 µm are recorded regularly (Kraft et al., 2021). The images were automatically classified following the methodology described in Kraft et al. (2022). Three morphotypes of filamentous cyanobacteria were identified: *Aphanizomenon* (comprising mostly *A. flosaquae*), *Dolichospermum* (mainly *Dolichospermum* species, but also including morphologically similar taxa, such as *Anabaenopsis, Cronbergia,* and *Anabaena* species), and *Nodularia* (containing all potential *Nodularia* species, such as *N. spumigena*).

Biovolumes were automatically estimated using the distance map method (Moberg and Sosik, 2012) and a conversion factor of 3.5 pixels/µm [determined using 6-µm standard beads (AlignFlow Plus, Molecular Probes, Inc.)]. Because pixel-based volumes tend to be overestimated for coiled filaments of *Dolichospermum* and *Nodularia*, these morphotypes were separated into straight and coiled forms, and specific conversion factors were applied to the coiled classes of both (Kraft et al., 2021; Kraft et al., 2025). Estimated biovolumes were converted to biomass (µg/L) by assuming a plasma density of 1 g/cm^3, as per CEN (2015).

2.2.4. Fluorescence measurements

Chl *a* fluorescence served as a proxy of total phytoplankton biomass and was measured using a Wetlabs ECO FLNTU fluorometer with an excitation/emission at 470/695 nm (Sea-Bird Scientific). The phycocyanin (PC) fluorescence, as a proxy for filamentous cyanobacterial biomass in the Baltic Sea, was measured using a MicroFlu-Blue fluorometer (TriOS Mess- und Datentechnik GmbH), with an excitation/emission at 620/655 nm (Seppälä et al., 2007). Both fluorometers are calibrated annually using algal and cyanobacterial cultures, respectively (Seppälä et al., 2021).

2.2.5. Nutrient and extracted Chl a measurements

Discrete samples for the analysis of dissolved inorganic nutrient concentrations ($NO_2^- + NO_3^-$, hereafter referred to as $NO_{2,3}$, and PO_4^{3-}, hereafter referred to as PO_4) and extracted Chl *a* concentrations were taken twice per month. In the EGF, the concentrations were averaged from samples collected at six stations along the route of SOOP *Finnmaid*. Sample collection at these stations was triggered at fixed longitudinal positions using an ISCO automated sampler. The samples were kept refrigerated in the dark until their analysis at the Syke laboratory (Raateoja et al., 2018). Nutrient concentrations were measured with a continuous flow analyzer (SAN++ series, Skalar) following the procedure developed by Hansen and Koroleff (1999). Chl *a* was extracted using 96% ethanol and measured fluorometrically following the standard procedure determined by HELCOM (2017).

2.3. Modeling of physical and meteorological parameters

To complement the surface-based SOOP observations, three-dimensional profiles of salinity and temperature, as well as wind speed at a 10-m height (U_{10m}) were derived from a numerical simulation of the Baltic Sea obtained using the General Estuarine Transport Model (GETM, Klingbeil and Burchard, 2013). The model setup employed a horizontal resolution of ~1 nautical mile (~1.8 km) and a vertical resolution of 60 adaptive terrain-following coordinate levels. A detailed description and comprehensive evaluation of the model are provided in studies by Gräwe et al. (2019) and Placke et al. (2018). Our study used the output from a model run that was reinitialized in 2003, driven by atmospheric forcing data from the German Weather Service's operational reanalysis (Zängl et al., 2015).

To assess the degree of stratification due to surface water warming

and integrate surface measurements over depth (Section 2.4.1), the mixed-layer depth (MLD, z_{mix}) was determined. Vertical temperature and salinity data from the model were used to calculate density profiles. The density differences ($\Delta\rho$) between consecutive depths were then determined, with the maximum density gradient defining the z_{mix} value, an indicator of the water column's thermohaline structure considered to represent the depth of active surface water mixing.

2.4. Quantification of N_2 fixation

2.4.1. CO_2 approach

Relative changes in C_T of the surface water, which indicate NCP, were derived from regional means of the pCO_2, SST, salinity, and alkalinity (A_T). The regional mean alkalinity was extracted from measurements within the Swedish National Monitoring Programme (SMHI, shark data base). Furthermore, temporal changes in alkalinity during the short-term production events were ignored in the calculation of the temporal changes in C_T. The calculation was performed using the CO2SYS software developed by Lewis and Wallace (1998), applying the carbonic acid dissociation constants (K_1 and K_2) from Millero (2010).

To estimate NCP based on the decrease in C_T, the effect of air-sea gas exchange, as a physical driver of CO_2 concentration changes, must be taken into account. This is particularly important given that surface water is strongly undersaturated in CO_2 due to ongoing organic matter (OM) production (Schneider et al. 2014a), and the relatively shallow summer mixed layer. The air-sea CO_2 flux ($F^{AS}_{CO_2}$) was calculated according to Eq. (1):

$$F^{AS}_{CO_2} = k_{660} \bullet \left(\frac{Sc}{660}\right)^{-0.5} \bullet k_0 \bullet \left(pCO_2^{atm} - pCO_2^{sea}\right), \quad (1)$$

where pCO_2^{sea} is the measured sea surface pCO_2, pCO_2^{atm} is the atmospheric pCO_2 (based on a fixed xCO_2 of 415 ppm), k_o is the temperature- and salinity-dependent solubility constant (Weiss, 1974), and Sc (Wanninkhof, 1992) is the Schmidt number of CO_2. The gas exchange transfer velocity for $Sc = 660$ (k_{660}) was determined using the quadratic wind speed (U_{10m})-dependent parametrization derived by Wanninkhof (2014), as shown in Eq. (2):

$$k_{660} = 0.251 \bullet U^2_{10m}. \quad (2)$$

Finally, NCP and associated N_2 fixation were derived from the temporal changes in C_T, while accounting for air-sea CO_2 exchange and the formation of dissolved organic carbon (DOC).

C_T depletion was determined based on the difference between the C_T concentration at the onset of the production period and the subsequent seasonal minimum. To estimate net organic carbon production (iC_{org}) over the entire time period, the change in C_T was integrated over the mean z_{mix} at the C_T minimum. The $F^{AS}_{CO_2}$ for these intervals was then added to the amount of C_T depletion to account for gas exchange. C_T, z_{mix}, and the variables used in Eqs. (1) and (2) were averaged over the respective study area. Furthermore, based on the assumption that DOC represents 20% of iC_{org} (Schneider et al., 2014a), this fraction was subtracted to estimate integrated particulate organic carbon production (iC_{POC}), representing a net empirical partitioning. N_2 fixation was quantified by accounting for the corresponding nitrogen demand, calculated by dividing iC_{POC} by the molar C/N ratio of POM. The latter was determined using monitoring data (IOW monitoring program) collected in July of each year from 2001 to 2014, yielding a mean value of 7.8 for the EGF. This approach was originally introduced and comprehensively described in a study by Schneider et al. (2014a). The use of different estimates of z_{mix} has been evaluated in Müller et al. (2021).

2.4.2. Quantification of biogeochemical effects: ΔN_2 and ΔO_2

Biogeochemically induced changes in N_2 and O_2 concentrations (ΔN_2 and ΔO_2) can be quantified by comparing the measured concentrations to controlled reference values representing the respective concentrations determined in the absence of biogeochemical processes and at a given temperature and salinity. These reference concentrations are not identical to saturation concentrations, as deviations may occur due to physical processes, such as delayed gas exchange after temperature-induced solubility changes. The ratio of the saturation concentration of a gas (X) and argon (Ar) is unchanged by physical processes, provided that X and Ar have identical physicochemical properties (Benson and Parker, 1961). The physically controlled reference concentration is then given by Eq. (3):

$$X_{phys} = \left(\frac{X}{Ar}\right)_{sat} \bullet Ar_{meas}, \quad (3)$$

where the subscripts "sat" and "meas" denote the saturation concentration and the measured concentration, respectively.

While the physicochemical properties of O_2 and Ar are largely similar, the temperature dependency of the solubility constants for N_2 and Ar distinctly differ. This discrepancy must be taken into account when interpreting biogeochemically induced changes in N_2, as small variations of ΔN_2, such as those associated with N_2 fixation, may lead to significant uncertainties (Schmale et al., 2019).

The biogeochemically induced deviation from the physically controlled reference concentration of a gas X (here, N_2 or O_2), ΔX, is given by Eq. (4):

$$\Delta X = X_{meas} - X_{phys}, \quad (4)$$

which together with Eq. (3) yields Eq. (5):

$$\Delta X = \left[\left(\frac{X}{Ar}\right)_{meas} - \left(\frac{X}{Ar}\right)_{sat}\right] \bullet Ar_{meas}. \quad (5)$$

3. Results and discussion

This study consisted of three steps, discussed in the following sections. First, a hotspot area of cyanobacteria and associated N_2 fixation was identified during the summer of 2023. Second, it was examined how this hotspot and its cyanobacterial bloom fit into the broader seasonal cycle of biological production. Third, both the bloom and N_2 fixation within the hotspot were investigated in detail, focusing on their intensity and temporal evolution in relation to significant biological, biogeochemical, and physical parameters.

For the interpretation of the data, all measurements obtained along each transect within the study area were averaged to derive a single representative value for this region.

3.1. Identification of the N_2 fixation hotspot area

The N_2 fixation hotspot was identified based on the derived C_T concentration. Fig. 2A shows the C_T values along the entire transect of the SOOP *Finnmaid* (see Fig. 1) for June and July 2023.

Since A_T values are higher in the southern than in the northern part of the transect, C_T values are generally higher in the south than in the north. Accordingly, at the beginning of June, C_T ranged from ~1650 μmol/kg in the Mecklenburg Bight (0–50 km, Fig. 2A) to ~1450 μmol/kg in the Gulf of Finland (900–1000 km). The first noticeable decrease in C_T across almost the entire transect began in mid-June and continued until early July, when C_T started to rise again. This decrease likely reflects biomass production by cyanobacteria, which meet their nitrogen demands through N_2 fixation. Therefore, a strong reduction in C_T per unit of time in a given area should indicate high N_2 fixation activity.

As shown in Fig. 2A, the largest decrease in C_T was observed along the transect between 850 and 1000 km, occurring at the end of June. This part of the transect also showed the most pronounced C_T signal throughout July. A satellite image from June 26 (Fig. 2B) revealed the

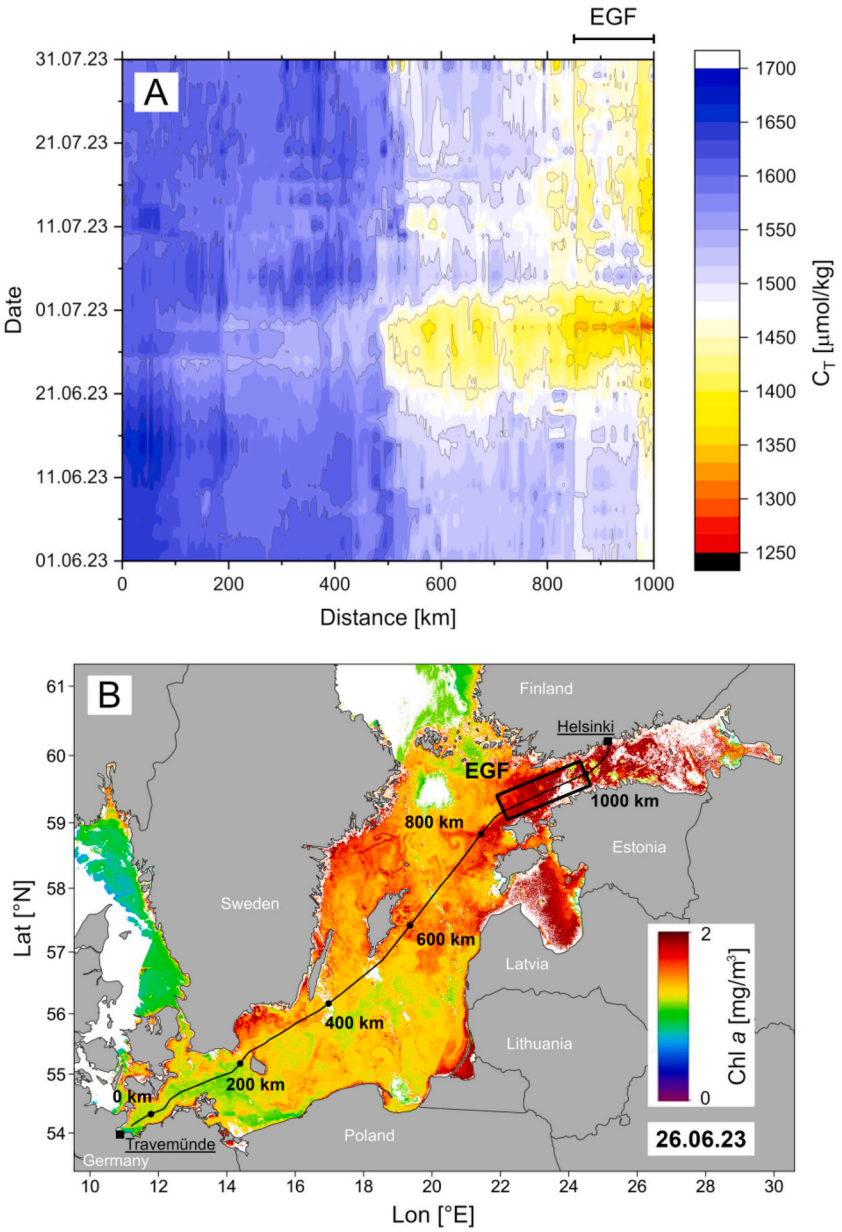


Fig. 2. (A) Hovmöller plot of C_T concentrations along the eastern transect of the *Finnmaid* (see Fig. 1) in June and July 2023. Missing values were linearly interpolated. (B) Sentinel-3 OLCI L2 satellite image, Open Water Channel was taken on June 26, 2023. The Algal pigment concentration in open waters estimates the surface Chl *a* concentrations. No data/clouds are indicated in white colour.

spatial extent and relative intensity of the surface bloom associated with cyanobacteria, showing a gradual intensification at ~500 km along the transect, with a distinct maximum also between 850 and 1000 km. The close mirroring of the bloom's spatial distribution and C_T identified this region as a hotspot of enhanced primary production, with a decrease further south. However, compared to calibrated sensor data (see Fig. 3B), the remote sensing product considerably underestimates Chl *a* concentrations and is therefore used solely for qualitative interpretation of bloom patterns. Based on these findings, our study focused on the section of the transect between 850 and 1000 km, defined as the EGF (Fig. 1 and 2B).

3.2. Seasonal dynamics of biogeochemical variables in the hotspot area

The seasonal cycle of biomass production in the central Baltic Sea, as inferred from CO_2 studies, was examined in detail by Schneider and Müller (2018). Their findings align well with the conditions in our studied hotspot area. The production dynamics determined in 2023 are described below.

At the beginning of the year, during the winter months of January and February, deep convective mixing in the EGF resulted in the transport of C_T and nutrients, such as $NO_{2,3}$ and PO_4, into the upper layers and thus in a vertical homogenization of the water column down to the permanent halocline (Fig. 3).

The C_T concentration in the EGF remained stable until April (Fig. 3A), when significant decrease took place due to spring phytoplankton bloom biomass production initiated by increasing solar radiation and shallowing of the surface mixed layer (Schneider and Müller, 2018). The concurrent increase in SST contributed to the development of a seasonal thermocline at depths of 10–20 m (Alenius et al., 1998). Consequently, vertical mixing was limited and the upper water layers were stabilized, trapping phytoplankton in the well-lit surface zone and facilitating their growth (Lass et al., 2010). This enhanced biological activity was also reflected by a rapid decline in the $NO_{2,3}$ and PO_4

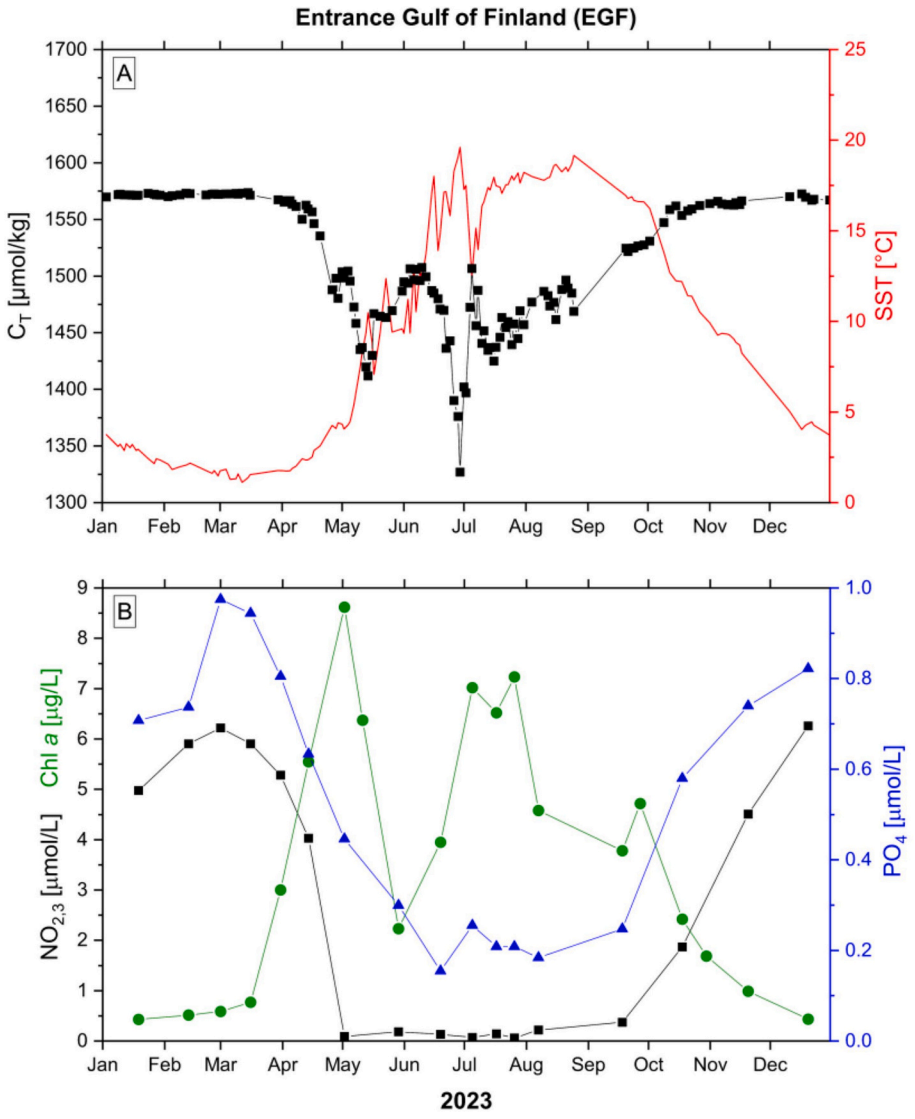


Fig. 3. Seasonal development of key biogeochemical variables in the surface waters of the EGF in 2023. (A) C_T concentrations (black squares) and sea surface temperatures (SST, red line). (B) The concentrations of extracted Chl *a* (green circles), nitrate plus nitrite ($NO_{2,3}$, black squares), and phosphate (PO_4, blue triangles). (For interpretation of the references to colour in this figure legend, the reader is referred to the web version of this article.)

concentrations, indicating the onset of the spring bloom, as evidenced both by the inorganic nutrient depletion and biomass accumulation (Fig. 3B). At the same time, the concentrations of extracted Chl *a* reached a maximum in early May (~ 9 µg/L) coinciding with the significant decrease in the C_T concentration, with a difference (ΔC_T) of ~175 µmol/kg by mid-May (Fig. 3A and B), confirming the occurrence of pronounced primary production. Nonetheless, despite the complete depletion of $NO_{2,3}$ by early May, C_T and PO_4 concentrations continued to decline, raising the question of which nitrogen source(s) sustained the ongoing production (Fig. 3A and B). The observed patterns could not be fully explained by a preferential remineralization of nitrogen-rich OM, dissolved organic nitrogen (DON) utilization, or shifts in macromolecular composition (Schneider and Müller, 2018). In previous studies, internal nitrogen storage pools in phytoplankton (Lignell et al., 2003) as well as external sources such as early "cold" N_2 fixation and nitrogen transport by migrating plankton have been proposed (Eggert and Schneider, 2015).

The spring bloom ended in mid-May and was followed by a period of low productivity known as the blue water phase (Schneider and Müller, 2018). The C_T signal, which behaves conservatively and is unaffected by temperature, did not reach a plateau during this period but instead increased slightly (Fig. 3A). This may have been due to a deepening of the thermocline, driven by stronger wind events and an intensified mixing with deeper water masses, that was unaffected by the preceding primary production and hosted the remineralization of OM, resulting in higher C_T concentrations (see Appendix A). This interpretation is supported by the fluctuating SST values recorded during May (Fig. 3A). Air-sea gas exchange also likely contributed to the C_T increase, as the surface water remained undersaturated with respect to CO_2. In addition, remineralization of the remaining spring bloom OM in the surface layer cannot be excluded. Consistent with the decline in biological activity during this period, the concentration of extracted Chl *a* decreased significantly until early June (Fig. 3B).

A second C_T minimum and extracted Chl *a* maximum, corresponding to the cyanobacterial bloom that was the focus of this study, occurred during the summer months of June and July (cf. Section 3.1). The decrease in the C_T concentration began on June 11 and coincided with a pronounced increase in SST, reaching up to ~21 °C (Fig. 3A). At this point, DIN had already been depleted for some time, as indicated by the $NO_{2,3}$ concentration, while minor amounts of residual PO_4 remained available (Fig. 3B). Numerous biological studies and field observations (e.g., Schmale et al., 2019; Schneider et al., 2014a; Wasmund et al.,

2001, 2005) have shown that this NCP is fueled by N_2 fixation. A comparison between the spring and summer blooms revealed the shorter duration of the latter, as after ~2 weeks the C_T concentration again increased. Multiple production pulses during a summer bloom are not uncommon (Müller et al., 2021; Kraft et al., 2025). In 2023, the EGF was characterized by a dominant production pulse at the end of June, followed by a less pronounced secondary pulse in July that indicated ongoing but reduced biological activity. The underlying cause is further explored in Section 3.3.2. The decrease in the C_T concentration during the main pulse, from ~1500 µmol/kg to ~1325 µmol/kg ($\Delta C_T \approx 175$ µmol/kg), corresponds approximately to the same ΔC_T observed during the spring bloom, despite slightly lower maximum concentrations of extracted Chl *a* (~7.5 µg/L) in summer. This apparent similarity in carbon drawdown can be explained by differences in pigment composition and cellular packaging between the two blooms: in summer, Chl *a* is typically contained in smaller cells with higher absorption efficiencies, and higher ambient light availability further enhances photosynthetic performance, allowing comparable productivity to be maintained with lower chlorophyll concentrations (Raateoja et al., 2004). By mid-June, PO_4 was nearly depleted, with mineralization processes, lateral mixing, and terrestrial inputs maintaining a remaining background concentration of <0.2 µmol/L (Fig. 3B). Notably, during N_2 fixation events, POM is characterized by very high C/P ratios (~500: Larsson et al., 2001; Nausch et al., 2008), while C/N ratios are close to the Redfield ratio (~7.5).

In autumn, decreasing surface temperatures and stronger winds triggered the gradual breakdown of thermal stratification, leading to increased vertical mixing. The deeper water masses, enriched in C_T and nutrients due to the remineralization of OM, contributed to a significant increase in the respective surface concentrations, while Chl *a* concentrations decreased due to the dilution of biomass in the mixed layer. As a result, all measured parameters reached levels similar to those at the beginning of the year, indicating the completion of the seasonal cycle (Schneider and Müller, 2018).

3.3. Evolution of the cyanobacterial bloom and N_2 fixation

Fig. 4 depicts the interactions between physical, biogeochemical, and biological processes, represented by key parameters, during the cyanobacterial bloom in the EGF in June and July 2023. Based on the temporal dynamics of the C_T concentration, three phases were identified: Phase 1 (shown in blue in Fig. 4), the period prior to the onset of the midsummer bloom, when C_T concentrations were relatively high and widely stable; phase 2, (green) the period of peak cyanobacterial activity, characterized by a significant decline in C_T and strong increase of e.g. filamentous cyanobacteria and phycocyanin; and phase 3 (orange), the post-bloom phase, when C_T concentrations gradually recovered to pre-bloom levels. These phases are discussed in detail in the following sections.

3.3.1. Pre-bloom conditions: phase 1

Phase 1 (01.06–11.06) marked the end of the blue water phase, characterized by low biological productivity and thus minimal changes in C_T concentrations (blue-shaded area in Fig. 4A). The slight variations in C_T mostly reflected day-night differences caused by the schedule of the SOOP *Finnmaid* (Section 2.1), with slightly lower C_T concentrations during the day due to light dependent primary production (see e.g. Honkanen et al., 2021). The increase in SST during phase 1, from ~9 °C to ~14 °C, was driven by the increased solar radiation (data not shown). Surface warming was enhanced by the steadily decreasing wind speeds (U_{10m}) to near-calm conditions (~1 m/s), resulting in reduced mixing of the upper water body and an intensified thermal stratification (Fig. 4B). This was evidenced by a progressive shallowing of the MLD (z_{mix}), which decreased from ~18 m to only 3 m by the end of phase 1.

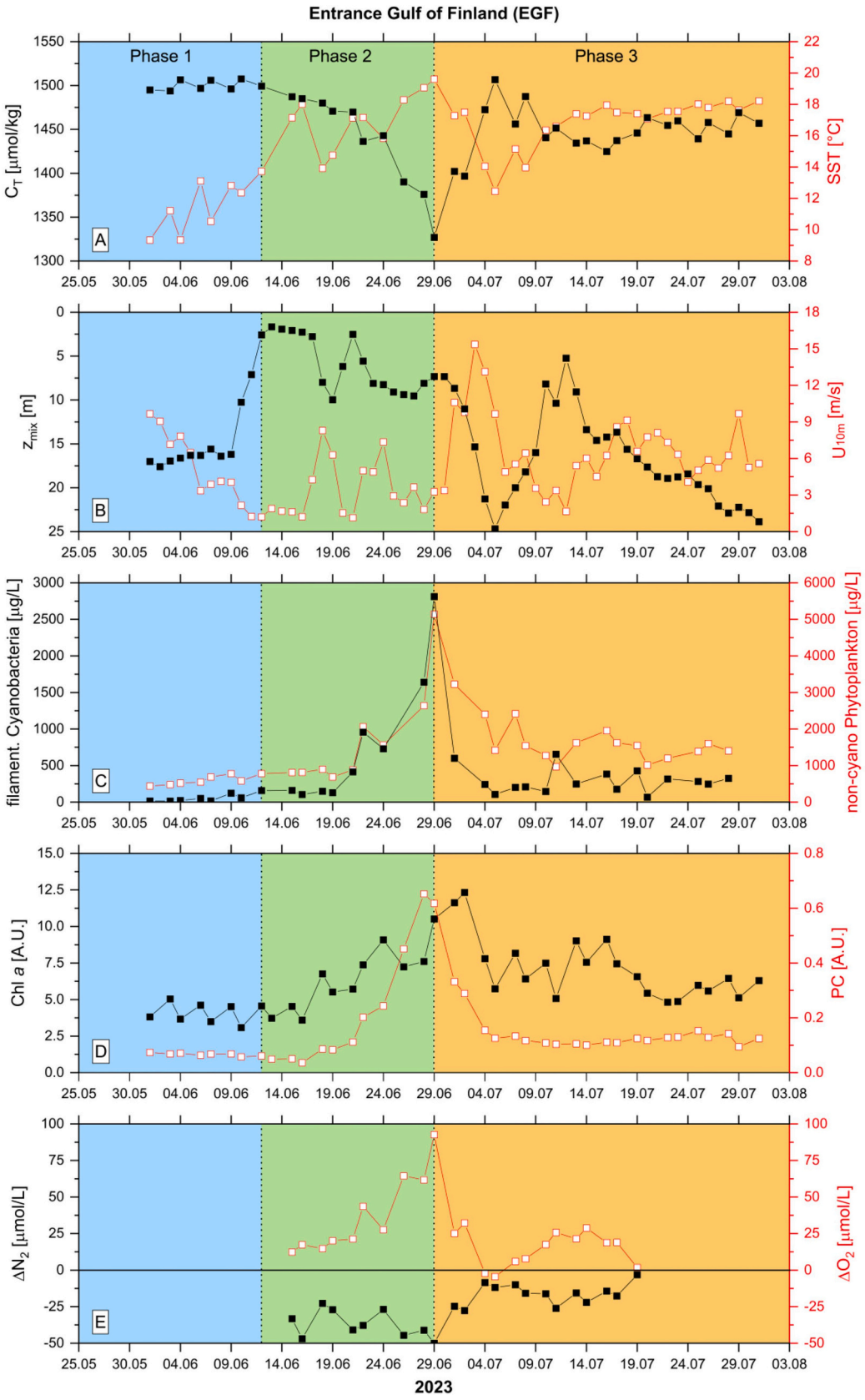
The temporal development of filamentous cyanobacteria was characterized by low biomass concentrations in early June, with only a slight increase, to ~125 µg/L, by the end of phase 1 (Fig. 4E). The biomass of non-cyanobacterial phytoplankton groups was also low (<500 µg/L). In terms of its composition, the phase 1 phytoplankton community consisted of small organisms (~70% of total biomass), with low contributions (≤35%) to the total biomass by dinoflagellates and filamentous cyanobacteria. The main filamentous species was *Aphanizomenon*, which, on average, accounted for >90% of the total filamentous cyanobacterial biomass (Fig. 5). This dominance can be attributed to its broader ecological niche and higher tolerance to lower temperatures compared to *Nodularia* and *Dolichospermum*, allowing it to proliferate earlier in the season (Suikkanen et al., 2010; Klawonn et al., 2016; Wasmund, 2017). Chl *a* fluorescence remained relatively low, with small fluctuations also attributable to the *Finnmaid*'s day-night measurement cycle in our study area, which alters in vivo fluorescence (Babin, 2008). Low Chl *a* concentrations have also been reported in the central Baltic Sea during early June, coinciding with nutrient depletion during the post-spring bloom period (Wasmund and Siegel, 2008). PC fluorescence was close to zero, indicating a negligible amount of cyanobacteria.

3.3.2. Cyanobacterial bloom initiation and maximum: phase 2

During phase 2 (12.6–29.6), representing the accumulation of cyanobacterial biomass in the EGF (green-shaded area in Fig. 4), C_T decreased by ~175 µmol/kg, from ~1500 µmol/kg to ~1325 µmol/kg (Fig. 4A). The decrease followed an exponential rather than a linear function, with ~70% of the total decline (~125 µmol/kg) occurring during the final 5 days of the bloom period (24.6–29.6). This pattern of C_T development can be explained by the abiotic conditions and the exponential growth of cyanobacteria, as outlined below.

The conditions at the beginning of phase 2 (12.6–16.6) were ideal for the initiation of a cyanobacterial bloom (Kahru et al., 2025), as they included a significant increase in SST of ~4 °C, shallow stratification (z_{mix}: 2.5 m), and calm weather (U10m: < 2 m/s) (Fig. 4A, B). However, the cyanobacteria bloom in the surface did not initiate immediately when the conditions were favorable, as indicated by the C_T data and the biomass of filamentous cyanobacteria (Fig. 4C). Even under favorable conditions, cyanobacterial gene expression, metabolism, and repair mechanisms require a period of acclimation before the maximum division rate is achievable (Wasmund, 2017), and a sufficient seed population is necessary. In addition, often the biomass starts to develop in the mixed water column and forms dense surface blooms only in the later phases (Stal et al., 2003). In 2023 environmental conditions varied after the initial warming of the SST, which increased from ~14 °C to ~20 °C, and two distinct temperature minima occurred, on June 18 and June 24. These sharp decreases of up to 4 °C suggested episodic mixing events that brought cooler, deeper waters to the surface. This interpretation was supported by the concurrent peaks in U_{10m}, which increased to 8 m/s, and by the increase in the MLD (z_{mix}) to a maximum of 10 m (Fig. 4B). The cooler SST, together with the disruption of a stable thermocline, likely hindered or temporarily suppressed biomass production. This becomes particularly evident between the wind events, on June 22, when SST, z_{mix}, and U_{10m} were favorable again for cyanobacterial growth, there was a noticeable decrease in C_T and a substantial increase in the biomass of filamentous cyanobacteria. The most intense period of CO_2 fixation and increased biomass production began after the second wind event (June 24)—when wind speeds remained low (< 4 m/s) for several days, SST increased steadily, and the abundance of cyanobacteria sufficed to allow significant population growth (Fig. 4A–C)—and continued until the end of phase 2. The importance of increasing SST in promoting and initiating cyanobacterial blooms has been reported in several studies (e.g., Lips and Lips, 2008; Schmale et al., 2019; Schneider et al., 2014a; Müller et al., 2021; Kahru et al., 2025). Fig. 6A shows the decrease in C_T with rising SST, the latter due to the increased solar irradiation efficiency at the low MLD.

The substantial cyanobacterial growth that occurred at the end of phase 2 may have been additionally supported by the vertical mixing caused by the two preceding wind events, which potentially entrained



(caption on next page)

Fig. 4. Temporal development in the EGF of (A) C_T and SST, (B) the mixed-layer depth (z_{mix}) and wind speed at 10 m height (U_{10m}), (C) biomass of filamentous cyanobacteria and non-cyanobacterial phytoplankton, (D) in vivo fluorescence of Chl *a* and phycocyanin (PC), where A.U. refers to arbitrary units, and (E) biogeochemically induced changes in N_2 and O_2 concentrations (ΔN_2 and ΔO_2) during June and July 2023. In each panel, the first-mentioned variable is represented by black filled squares connected by a black line, and the second-mentioned variable by red open squares connected by a red line. Shaded areas indicate the different phases of the bloom: blue (phase 1), green (phase 2), and orange (phase 3) as discussed in the text. (For interpretation of the references to colour in this figure legend, the reader is referred to the web version of this article.)

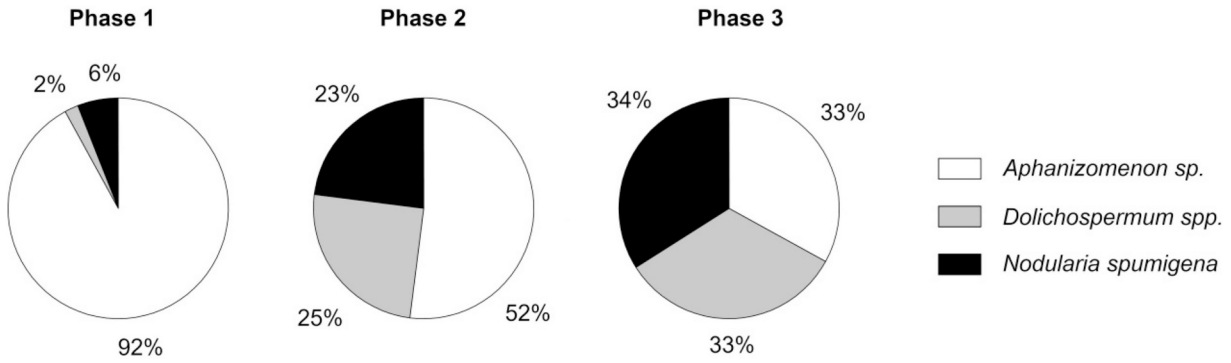


Fig. 5. Average biomass proportions of the three main filamentous cyanobacteria species during each phase of the bloom in the EGF.

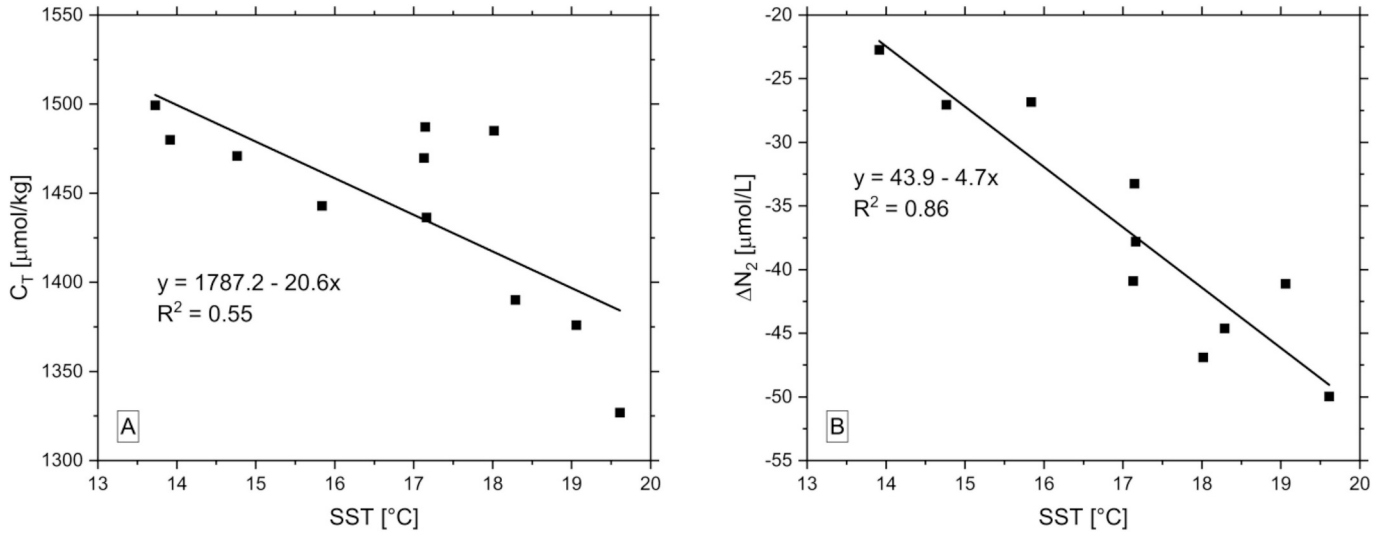


Fig. 6. Relationship between SST and C_T (A), and the biogenic changes in the N_2 concentration (ΔN_2) (B) during phase 2. The equation and coefficient of determination (R^2) refer to the black regression line.

PO_4 from deeper waters and prevented PO_4 limitation (Kononen et al., 1996; see Appendix A).

Based on the C_T decrease (~175 µmol/kg) and the mean MLD at the C_T minimum (~7.3 m), we calculated the depth-integrated C_T loss (iC_T) to 1.28 mol/m^2. The contribution of air-sea gas exchange, calculated as described in Section 2.4.1, was 0.11 mol/m^2. Together with iC_T, this resulted in an iC_{org} of 1.39 mol/m^2, with gas exchange contributing less than 8%. Since we estimate 20% of iC_{org} to consist of DOC, iC_{POC} was 1.11 mol/m^2. Based on the C/N ratio of the POM (7.8, Section 2.4.1), this corresponds to a nitrogen demand of ~143 mmol/m^2, primarily met by cyanobacterial N_2 fixation because DIN was depleted by early May (Fig. 3B), and the estimated contribution from atmospheric deposition (0.1 mmol/m^2•day; Bartnicki et al., 2011; HELCOM, 2024) was negligible. Schneider et al. (2014a) used the same approach in a region of the northeastern Gotland Basin in 2005, 2008, 2009, and 2011, obtaining mean values of iC_{POC} and N_2 fixation of 1.06 mol/m^2 and 138 mmol/m^2, respectively. Thus, midsummer production in the EGF in 2023 closely matched that reported for previous years in the northeastern Gotland Basin.

During phase 2, the biomass of filamentous cyanobacteria increased from ~250 µg/L to nearly 3000 µg/L; the latter accounted for >35% of total phytoplankton biomass (Fig. 4C). The biomass of all three filamentous species increased, with *Aphanizomenon* contributing ~50% to filamentous cyanobacterial biomass, while the contributions of *Dolichospermum* and *Nodularia* increased to ~25% each (Fig. 5). The biomass of non-cyanobacterial phytoplankton (mostly small unidentified organisms) also increased, from roughly 500 µg/L to 5000 µg/L, and followed a temporal pattern identical to that of filamentous cyanobacteria (Fig. 4C). This suggests that non-cyanobacterial phytoplankton benefited from the bloom due to its release of bioavailable nitrogen into the environment through N_2 fixation (Adam et al., 2016).

Fluorescence measurements confirmed the occurrence of a cyanobacterial bloom. The temporal evolution of PC and Chl *a* was characterized by concurrent increases (Fig. 4D) and aligned well with the C_T concentration and biomass. However, in vivo Chl *a* fluorescence is not a reliable proxy for cyanobacteria, but instead primarily represents the presence of non-cyanobacterial phytoplankton groups (Kraft et al., 2025; Seppälä et al., 2007).

The role of N_2 fixation in enabling the observed production event was further explored by evaluating the accompanying biogenic changes in N_2 and O_2. During the period of maximum production, ΔO_2 reached a maximum of ~90 μmol/kg, which coincided with the minimum of C_T (Fig. 4E) and corresponded to a biologically induced O_2 saturation of >130%. The extreme O_2 oversaturation was plausible given the extremely low pCO_2 (~60 μatm) during the production peak. The consistently negative ΔN_2 values during phase 2 indicated N_2 undersaturation of the surface water, with values as low as ~90%. The corresponding N_2 loss implied an unrealistically high rate of N_2 fixation and was considered an artifact, attributable to the differences in the temperature coefficients of the solubility constants of N_2 and Ar (see "Fundamentals and Limitations of the N_2/Ar Method" in Schmale et al., 2019). The values for ΔN_2 were therefore treated as qualitative indicators of the N_2 saturation state. N_2 undersaturation was evidenced by the consistently low ΔN_2 values, with the minimum ΔN_2 coinciding with both the C_T minimum and the maximum cyanobacterial biomass on June 29 (Fig. 4E). These findings further supported our conclusion that summer production in the EGF was fueled by cyanobacterial N_2 fixation. In addition, the temporally inverse pattern of ΔN_2 relative to ΔO_2, together with its concurrent decline in C_T, highlighted the tight coupling between biomass production through photosynthesis and N_2 fixation. This relationship was also demonstrated by the correlation between ΔN_2 and SST, as reported in previous studies (e.g., Schmale et al., 2019). Fig. 6B shows that N_2 depletion due to N_2 fixation was closely related to the rise in SST. Together with the results shown in Fig. 6A, these observations indicate that the cyanobacterial bloom and the associated N_2 fixation became more pronounced as long as the SST did not decrease.

3.3.3. Post-bloom dynamics: phase 3

Phase 3 (30.06–31.07), corresponding to the post-bloom period, was initiated by a strong wind event. As shown in Fig. 4B, wind speed (U_{10m}) increased significantly after June 29, reaching a peak of ~15 m/s on July 3. This resulted in vertical mixing, with z_{mix} deepening from ~7.5 m to 25 m.

After July 3, wind speeds decreased again but remained, on average, higher than during phase 2. The reduced wind intensities (<4 m/s) allowed for temporary restratification such that, by July 12, the MLD was again ~5 m. Thereafter, the increasing wind speeds returned the MLD to ~25 m (Fig. 4B).

The sudden high wind speeds and resulting vertical mixing caused a sharp drop in the SST (Fig. 4A), from almost 20 °C to 12 °C. The surface salinity increased from approximately 6 PSU before the mixing event (Phase 1 and 2) to ~6.5 PSU afterwards. The wind event and its associated effects downgraded primary production and brought up deeper water masses less affected by CO_2 uptake and therefore richer in C_T (see Appendix A). Consequently, the C_T concentration increased significantly, by ~175 μmol/kg, approximating pre-bloom levels. Following the peak wind event on July 3, SST gradually increased again, to ~18 °C. C_T then temporarily decreased by up to 75 μmol/kg, reaching a minimum on July 15. However, compared to productivity during phase 2, this was a minor episode (Fig. 4A). However, it must be taken into account that at the same time the MLD increased, which means that the depth-integrated NCP might not be as low as suggested by the surface decrease in C_T. After July 15, C_T values began to rise again, and no further productive phase was identified.

The same trends were seen in the IFCB measurements and provided additional support for the patterns in the C_T data (Fig. 4C). With the onset of the wind event, the biomass of both filamentous cyanobacteria and non-cyanobacterial phytoplankton began to decline sharply, as vertical mixing diluted the surface layer such that growth conditions were no longer favorable, consistent with observations by Kraft et al. (2021). On July 11, following the temporary re-stratification of the water column after the wind event, the abundance of filamentous cyanobacteria increased briefly, to ~500 μg/L. The absence of a further significant increase indicated the end of the bloom. Throughout phase 3, all three filamentous species contributed equally to the biomass of filamentous cyanobacteria (Fig. 5). By contrast, the increase in the biomass of non-cyanobacterial phytoplankton, which began around July 11, was gradual and reached a peak of ~1000 μg/L by July 16. However, for both groups, growth was minor in the surface water compared to the substantial increase during phase 2, consistent with the C_T dynamics shown in Fig. 4A.

This dynamic was also apparent from the fluorescence data, which showed marked declines in PC and Chl *a* fluorescence, although the levels of both were slightly higher than during phase 1. The Chl *a* fluorescence level indicated that the minor production in phase 3 was largely driven by non-cyanobacterial phytoplankton.

The ΔN_2 and ΔO_2 values (Fig. 4E) confirmed the described sequence of events by showing a clear decline in cyanobacterial productivity due to the wind event. ΔN_2 increased, indicating no biogenic changes, until July 4, while the slightly negative ΔO_2 marked the upwelling of deeper waters in which mineralization processes had consumed oxygen. This upwelling likely also supplied nutrients to the surface layer, which, however, did not accumulate in the observations (Fig. 3B), indicating their rapid uptake by non-cyanobacterial phytoplankton. The subsequent decline in ΔN_2 indicated renewed N_2 fixation, with the minimum coinciding with the increase in filamentous cyanobacteria biomass on July 11. The ΔO_2 data showed a corresponding rise in O_2 production, which reached a maximum on July 14. However, these biogenic concentration changes were much smaller than those that marked phase 2. Finally, both ΔN_2 and ΔO_2 gradually returned to zero, indicating the decline of bloom-related activity and thus bloom termination.

4. Summary

This study combined continuous, high-resolution measurements of biological and biogeochemical parameters along a ferry route across the Baltic Sea with modeled physical parameters to investigate the composition of the cyanobacterial community and their impact on the biogeochemistry of the surface water. Our multi-method approach enabled a comprehensive assessment of the timing, magnitude, and drivers of these blooms.

Key findings include: (i) the majority (70%) of the C_T decline from the main cyanobacterial primary production pulse occurred within a short (5-day) window; (ii) C_T drawdown was clearly linked to N_2 fixation, evidenced by direct N_2 measurements (ΔN_2) and phytoplankton community analyses; (iii) determinations of C_T dynamics and filamentous cyanobacterial biomass indicated that rapid population growth was preceded by an acclimation phase; and (iv) cyanobacterial N_2 fixation provided a nitrogen source that enabled the growth of non-cyanobacterial phytoplankton.

Quantitative assessments of biologically induced concentration changes due to N_2 fixation were not possible using ΔN_2, as differences in the temperature coefficients of the solubility constants of N_2 and Ar introduced substantial errors. However, ΔN_2 was highly valuable for qualitative interpretations, because the observed N_2 undersaturation in surface waters is most consistently explained by N_2 fixation under the prevailing stratified, DIN-depleted conditions.

CRediT authorship contribution statement

Sören Iwe: Writing – review & editing, Writing – original draft, Methodology, Investigation, Formal analysis, Data curation, Conceptualization. **Bernd Schneider:** Writing – review & editing, Methodology, Data curation, Conceptualization. **Lumi Haraguchi:** Writing – review & editing, Investigation, Data curation. **Kaisa Kraft:** Writing – review & editing, Investigation, Data curation. **Gregor Rehder:** Writing – review & editing, Resources. **Jukka Seppälä:** Writing – review & editing, Resources, Data curation. **Ulf Gräwe:** Writing – review & editing, Resources, Data curation. **Carsten Mönnig:** Writing – review & editing, Resources. **Oliver Schmale:** Writing – review & editing, Methodology,

Investigation, Conceptualization.

Funding

The Operation of DE-SOOP-Finnmaid has been supported by funding through the German support of the ICOS RI through the German Federal Ministries of Science, Technology and Space (BMFTR) and Transport (BMV). This study utilized research infrastructure as part of FINMARI (Finnish Marine Research Infrastructure consortium) and CSC – IT Center for Science, Finland, for computational resources. LH was supported by OBAMA-NEXT (Grant Agreement No 101081642), funded by the European Union under the Horizon Europe program. KK was supported by the Research Council of Finland project FASTVISION-plus (Grant no 339355). SI, OS, and BS were supported by the German Research Foundation (grant. Nos. SCHM 2530/8-1 and SCHN 582/9-1).

Declaration of competing interest

The authors declare that the research was conducted in the absence of any commercial or financial relationships that could be construed as a potential conflict of interest.

Acknowledgements

We acknowledge Bernd Sadkowiak, Michael Glockzin, Stefan Otto, Petri Maunula, Sami Kielosto and Pasi Ylöstalo for support during the construction, build up and maintenance of the instrumentation on SOOP Finnmaid. We thank InProcess Instruments (IPI) and the crew of the Finnmaid for their generous support.

Appendix A. Vertical water column profile in the hotspot area

The vertical water profile presented in Fig. A.1 was recorded on 22 July 2023 (end of Phase 3) during the EMB (Elisabeth Mann Borgese) Expedition No. 322. For detailed information on the cruise and the methods applied, please refer to the official cruise report (Schmale et al., 2023). The profile was obtained at Station T21 (59.719°N, 24.065°E), located in the cyanobacterial hotspot defined in this study, at the entrance to the Gulf of Finland (EGF).

Fig. A.1 shows the vertical distribution of the C_T and PO_4 concentrations, which describe the biogeochemical properties of the water column, as well as the temperature and salinity, which represent its physical characteristics. The mixed layer depth (z_{mix} = 13.23 m), calculated from the latter parameters as described in Section 2.3, is positioned just above the thermocline. Within the mixed layer, the water mass is highly homogeneous, showing only minor variations in any of the parameters, while PO_4 is nearly depleted due to preceding biological production. Below the mixed layer, C_T and PO_4 concentrations increase steadily with depth. While the increase in PO_4 reflects remineralization processes of organic matter (OM) produced in surface waters, the increase in C_T is also driven by increasing salinity and the associated rise in alkalinity. Concurrently, temperature decreases to values around 4 °C, while salinity increases with depth.

A wind-induced mixing event can deepen the mixed layer and bring deeper water to the surface, increasing surface C_T and PO_4 concentrations.

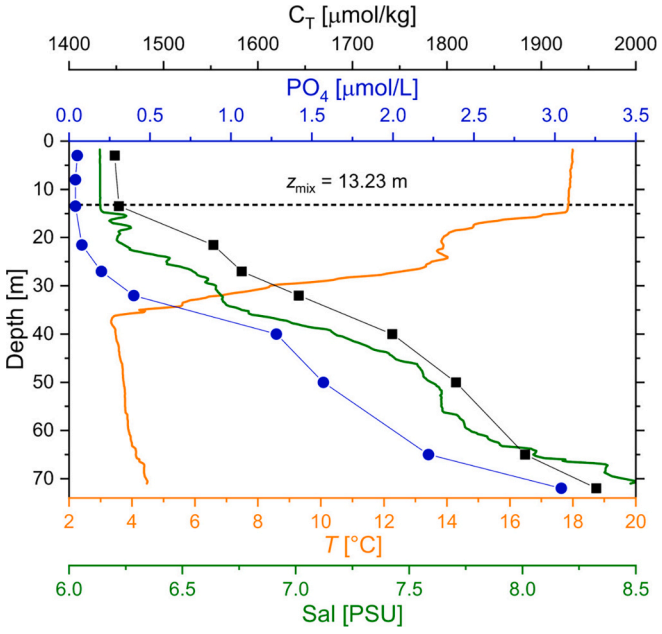


Fig. A.1: Vertical profile of C_T (black squares), phosphate concentration (PO_4, blue circles), temperature (*T*, orange line), and salinity (Sal, green line) measured at Station T21 (59.719°N, 24.065°E) on 22 July 2023 during the EMB Expedition No. 322. The black dashed horizontal line indicates the mixed layer depth (z_{mix} = 13.23 m). (For interpretation of the references to colour in this figure legend, the reader is referred to the web version of this article.)

Data availability

Research Link Provided (Iwe et al., 2026)

Coupled Biogeochemical, Biological, and Physical Controls on Nitrogen Fixation during a Cyanobacterial Bloom in the Baltic Sea (Original data) (IOW publications)

References

Adam, B., Klawonn, I., Svedén, J.B., Bergkvist, J., Nahar, N., Walve, J., Littmann, S., Whitehouse, M.J., Lavik, G., Kuypers, M.M.M., Ploug, H., 2016. N2-fixation, ammonium release and N-transfer to the microbial and classical food web within a plankton community. ISME J. 10, 450–459. https://doi.org/10.1038/ismej.2015.126.

Alenius, P., Myrberg, K., Nekrasov, A., 1998. The physical oceanography of the Gulf of Finland: a review. Boreal Environ. Res. 3, 97–125. ISSN 1239-6095.
Babin, M., 2008. Phytoplankton fluorescence theory, current literature and in situ measurement. In: Babin, M., Roesler, C.S., Cullen, J.J. (Eds.), Real-Time Coastal Observing Systems for Marine Ecosystem Dynamics and Harmful Algal Blooms: Theory, Instrumentation and Modeling. Unesco, Paris, pp. 237–280.
Benson, B. B. and Parker, P. D. M.: Nitrogen/argon and nitrogen isotope ratios in aerobic sea water, Deep-Sea Res. (1953), 7, 237–253, doi:https://doi.org/10.1016/0146-6313(61)90042-9, 1961.
Bartnicki, J., Semeena, V.S., Fagerli, H., 2011. Atmospheric deposition of nitrogen to the Baltic Sea in the period 1995–2006. Atmos. Chem. Phys. 11, 10057–10069. https://doi.org/10.5194/acp-11-10057-2011.
CEN, 2015. DIN EN 16695 water quality – guidance on the estimation of phytoplankton biovolume: english version EN 16695:2015.
Eggert, A., Schneider, B., 2015. A nitrogen source in spring in the surface mixed-layer of the Baltic Sea: evidence from total nitrogen and total phosphorus data. J. Mar. Syst. 148, 39–47. https://doi.org/10.1016/j.jmarsys.2015.01.005.
Gräwe, U., Klingbeil, K., Kelln, J., Dangendorf, S., 2019. Decomposing mean sea level rise in a semi-Enclosed Basin, the Baltic Sea. J. Clim. 32, 3089–3108. https://doi.org/10.1175/JCLI-D-18-0174.1.
Gülzow, W., Rehder, G., Schneider, B., Deimling, J.S., Sadkowiak, B., 2011. A new method for continuous measurement of methane and carbon dioxide in surface waters using off-axis integrated cavity output spectroscopy (ICOS): an example from the Baltic Sea. Limnol. Oceanogr. Methods 9, 176–184. https://doi.org/10.4319/lom.2011.9.176.
Gülzow, W., Rehder, G., Schneider, V., Deimling, J., Seifert, T., Tóth, Z., 2013. One year of continuous measurements constraining methane emissions from the Baltic Sea to the atmosphere using a ship of opportunity. Biogeosciences 10, 81–99. https://doi.org/10.5194/bg-10-81-2013.
Hamme, R.C., Emerson, S.R., 2004. The solubility of neon, nitrogen and argon in distilled water and seawater. Deep-Sea Res. I Oceanogr. Res. Pap. 51, 1517–1528. https://doi.org/10.1016/j.dsr.2004.06.009.
Hansen, H.P., Koroleff, F., 1999. Determination of nutrients. In: Methods of Seawater Analysis. John Wiley & Sons, Ltd, pp. 159–228. https://doi.org/10.1002/9783527613984.ch10.
HELCOM, 2017. Manual for marine monitoring in the COMBINE program of HELCOM. . Last updated 2017. https://helcom.fi/wp-content/uploads/2020/02/Manual-for-Marine-Monitoring-in-the-COMBINE-Programme-of-HELCOM.pdf (accessed 03 February 2026).
HELCOM, 2021a. Analysis of Total Nitrogen in the Baltic Sea and Implications for Time Lag in Achieving Good Environmental Status (GES). https://helcom.fi/wp-content/uploads/2021/11/Analysis-of-total-nitrogen-in-the-Baltic-Sea-and-implications-for-time-lag-in-achieving-good-environmental-status-GES.pdf (accessed 07 November 2025).
HELCOM, 2021b. Background Information on the Baltic Sea Catchment Area for the seventh Baltic Sea Pollution load Compilation (PLC-7). https://helcom.fi/wp-content/uploads/2021/12/Background-information-on-the-Baltic-Sea-catchment area-for-the-Seventh-Baltic-Sea-Pollution-load-compilation-PLC-7-211202.pdf.
HELCOM, 2024. Atmospheric Nitrogen Deposition to the Baltic Sea. HELCOM Baltic Sea Environment Fact Sheets 2024. Online. https://helcom.fi/wp-content/uploads/2025/02/Atmospheric-nitrogen-deposition-to-the-Baltic-Sea_2024.pdf (accessed 07 November 2025).
Honkanen, M., Müller, J.D., Seppälä, J., Rehder, G., Kielosto, S., Ylöstalo, P., Mäkelä, T., Hatakka, J., Laakso, L., 2021. The diurnal cycle of pCO_2 in the coastal region of the Baltic Sea. Ocean Sci. 17, 1657–1675. https://doi.org/10.5194/os-17-1657-2021.
Iwe, S., Schmale, O., Schneider, B., 2025. Technical note: testing a new approach for the determination of N_2 fixation rates by coupling a membrane equilibrator to a mass spectrometer for long-term observations. Biogeosciences 22, 1767–1779. https://doi.org/10.5194/bg-22-1767-2025.
Kahru, M., Cahill, B., Elmgren, R., Rehder, G., 2025. What initiates cyanobacterial blooms in the Baltic Sea? Harmful Algae 148, 102924. https://doi.org/10.1016/j.hal.2025.102924.
Kaitala, S., Seppälä, J., Raateoja, M., Hällfors, S., Fleming-Lehtinen, V., Maunula, P., Helminen, J., Ylöstalo, P., 2008. In: Recent Advances in Ferrybox Monitoring on Board Finnmaid Ferry. 2008 IEEE/OES US/EU-Baltic International Symposium, pp. 1–5. https://doi.org/10.1109/BALTIC.2008.4625504.
Karjalainen, M., Engström-Öst, J., Korpinen, S., Peltonen, H., Pääkkönen, J.-P., Rönkkönen, S., Suikkanen, S., Viitasalo, M., 2007. Ecosystem consequences of cyanobacteria in the northern Baltic Sea. Ambio 36, 195–202. https://doi.org/10.1579/0044-7447(2007)36[195:ECOCIT]2.0.CO;2.
Klawonn, I., Nahar, N., Walve, J., Andersson, B., Olofsson, M., Svedén, J.B., Littmann, S., Whitehouse, M.J., Kuypers, M.M.M., Ploug, H., 2016. Cell-specific nitrogen- and carbon-fixation of cyanobacteria in a temperate marine system (Baltic Sea). Environ. Microbiol. 18, 4596–4609. https://doi.org/10.1111/1462-2920.13557.
Klingbeil, K., Burchard, H., 2013. Implementation of a direct nonhydrostatic pressure gradient discretisation into a layered ocean model. Ocean Model 65, 64–77. https://doi.org/10.1016/j.ocemod.2013.02.002.
Kononen, K., Kuparinen, J., Mäkelä, K., Laanemets, J., Pavelson, J., Nõmmann, S., 1996. Initiation of cyanobacterial blooms in a frontal region at the entrance to the Gulf of Finland, Baltic Sea. Limnol. Oceanogr. 41, 98–112. https://doi.org/10.4319/lo.1996.41.1.0098.
Kraft, K., Seppälä, J., Hällfors, H., Suikkanen, S., Ylöstalo, P., Anglès, S., Kielosto, S., Kuosa, H., Laakso, L., Honkanen, M., Lehtinen, S., Oja, J., Tamminen, T., 2021. First application of IFCB high-frequency imaging-in-flow cytometry to investigate bloom-forming filamentous Cyanobacteria in the Baltic Sea. Front. Mar. Sci. 8. https://doi.org/10.3389/fmars.2021.594144.
Kraft, K., Velhonoja, O., Eerola, T., Suikkanen, S., Tamminen, T., Haraguchi, L., Ylöstalo, P., Kielosto, S., Johansson, M., Lensu, L., Kälviäinen, H., Haario, H., Seppälä, J., 2022. Towards operational phytoplankton recognition with automated high-throughput imaging, near-real-time data processing, and convolutional neural networks. Front. Mar. Sci. 9. https://doi.org/10.3389/fmars.2022.867695.
Kraft, K., Haraguchi, L., Hällfors, H., Suikkanen, S., Ylöstalo, P., Kielosto, S., Skyttä, A., Laakso, L., Honkanen, M., Kahru, M., Seppälä, J., 2025. Monitoring cyanobacteria blooms with complementary measurements – a similar story told using high-throughput imaging, optical sensors, light microscopy, and satellite-based methods. Harmful Algae 147, 102865. https://doi.org/10.1016/j.hal.2025.102865.
Larsson, U., Hajdu, S., Walve, J., Elmgren, R., 2001. Baltic Sea nitrogen fixation estimated from the summer increase in upper mixed layer total nitrogen. Limnol. Oceanogr. 46, 811–820. https://doi.org/10.4319/lo.2001.46.4.0811.
Lass, H.-U., Mohrholz, V., Nausch, G., Siegel, H., 2010. On phosphate pumping into the surface layer of the eastern Gotland Basin by upwelling. J. Mar. Syst. 80, 71–89. https://doi.org/10.1016/j.jmarsys.2009.10.002.
Lewis, E.R., Wallace, D.W.R., 1998. Program Developed for CO2 System Calculations, Environmental System Science Data Infrastructure for a Virtual Ecosystem (ESS-DIVE) (United States). https://doi.org/10.15485/1464255.
Liblik, T., Lips, U., 2019. Stratification has strengthened in the Baltic Sea – an analysis of 35 years of observational data. Front. Earth Sci. 7. https://doi.org/10.3389/feart.2019.00174.
Lignell, R., Seppälä, J., Kuuppo, P., Tamminen, T., Andersen, T., Gismervik, I., 2003. Beyond bulk properties: responses of coastal summer plankton communities to nutrient enrichment in the northern Baltic Sea. Limnol. Oceanogr. 48, 189–209. https://doi.org/10.4319/lo.2003.48.1.0189.
Lips, I., Lips, U., 2008. Abiotic factors influencing cyanobacterial bloom development in the Gulf of Finland (Baltic Sea). Hydrobiologia 614, 133–140. https://doi.org/10.1007/s10750-008-9449-2.
Millero, F.J., 2010. Carbonate constants for estuarine waters. Mar. Freshw. Res. 61, 139–142. https://doi.org/10.1071/MF09254.
Moberg, E.A., Sosik, H.M., 2012. Distance maps to estimate cell volume from two-dimensional plankton images. Limnol. Oceanogr. Methods 10, 278–288. https://doi.org/10.4319/lom.2012.10.278.
Montoya, J.P., Voss, M., Kahler, P., Capone, D.G., 1996. A simple, high-precision, high-sensitivity tracer assay for N(inf2) fixation. Appl. Environ. Microbiol. 62, 986–993. https://doi.org/10.1128/aem.62.3.986-993.1996.
Müller, J.D., Schneider, B., Gräwe, U., Fietzek, P., Wallin, M.B., Rutgersson, A., Wasmund, N., Krüger, S., Rehder, G., 2021. Cyanobacteria net community production in the Baltic Sea as inferred from profiling pCO2 measurements. Biogeosciences 18, 4889–4917. https://doi.org/10.5194/bg-18-4889-2021.
Nausch, M., Nausch, G., Wasmund, N., Nagel, K., 2008. Phosphorus pool variations and their relation to cyanobacteria development in the Baltic Sea: a three-year study. J. Mar. Syst. 71, 99–111. https://doi.org/10.1016/j.jmarsys.2007.06.004.
Olson, R.J., Sosik, H.M., 2007. A submersible imaging-in-flow instrument to analyze nano-and microplankton: imaging FlowCytobot. Limnol. Oceanogr. Methods 5, 195–203. https://doi.org/10.4319/lom.2007.5.195.
O'Neil, J.M., Davis, T.W., Burford, M.A., Gobler, C.J., 2012. The rise of harmful cyanobacteria blooms: the potential roles of eutrophication and climate change. Harmful Algae 14, 313–334. https://doi.org/10.1016/j.hal.2011.10.027.
Placke, M., Meier, H.E.M., Gräwe, U., Neumann, T., Frauen, C., Liu, Y., 2018. Long-term mean circulation of the Baltic Sea as represented by various ocean circulation models. Front. Mar. Sci. 5. https://doi.org/10.3389/fmars.2018.00287.
Raateoja, M., Seppälä, J., Kuosa, H., 2004. Bio-optical modelling of primary production in the SW Finnish coastal zone, Baltic Sea: fast repetition rate fluorometry in case 2 waters. Mar. Ecol. Prog. Ser. 267, 9–26. https://doi.org/10.3354/meps267009.
Raateoja, M., Hällfors, H., Kaitala, S., 2018. Vernal phytoplankton bloom in the Baltic Sea: intensity and relation to nutrient regime. J. Sea Res. 138, 24–33 doi:0.1016/j.seares.2018.05.003.
Rolff, C., Almesjö, L., Elmgren, R., 2007. Nitrogen fixation and abundance of the diazotrophic cyanobacterium Aphanizomenon sp. in the Baltic proper. Mar. Ecol. Prog. Ser. 332, 107–118. https://doi.org/10.3354/meps332107.
Salihoglu, B., Neuer, S., Painting, S., Murtugudde, R., Hofmann, E.E., Steele, J.H., Hood, R.R., Legendre, L., Lomas, M.W., Wiggert, J.D., Ito, S., Lachkar, Z., Hunt, G.L., Drinkwater, K.F., Sabine, C.L., 2013. Bridging marine ecosystem and biogeochemistry research: lessons and recommendations from comparative studies. J. Mar. Syst. 109-110, 161–175. https://doi.org/10.1016/j.jmarsys.2012.07.005.
Schmale, O., Karle, M., Glockzin, M., Schneider, B., 2019. Potential of nitrogen/argon analysis in surface waters in the examination of areal nitrogen deficits caused by nitrogen fixation. Environ. Sci. Technol. 53, 6869–6876. https://doi.org/10.1021/acs.est.8b06665.
Schmale, O., Bauersachs, T., Brüchert, V., Cotovicz Jr., L.C., Gehm, C., Glockzin, M., Haraguchi, L., Iwe, S., Kolbe, M., Marquez Lencina Avila, J., Rehder, G., 2023. Nitrogen Fixation and Production in the Baltic Proper (Baltic Sea), Cruise No. EMB322, July 14–July 31, 2023, Rostock (Germany) - Rostock (Germany). https://doi.org/10.48433/CR_EMB322.
Schneider, B., Müller, J.D., 2018. Biogeochemical transformations in the Baltic Sea. springer international publishing, Cham. https://doi.org/10.1007/978-3-319-61699-5.
Schneider, B., Gustafsson, E., Sadkowiak, B., 2014a. Control of the mid-summer net community production and nitrogen fixation in the Central Baltic Sea: an approach based on pCO2 measurements on a cargo ship. J. Mar. Syst. 136, 1–9. https://doi.org/10.1016/j.jmarsys.2014.03.007.
Schneider, B., Gülzow, W., Sadkowiak, B., Rehder, G., 2014b. Detecting sinks and sources of CO2 and CH4 by ferrybox-based measurements in the Baltic Sea: three

case studies. J. Mar. Syst. 140, 13–25. https://doi.org/10.1016/j.jmarsys.2014.03.014.
Schneider, B., Buecker, S., Kaitala, S., Maunula, P., Wasmund, N., 2015. Characteristics of the spring/summer production in the Mecklenburg bight (Baltic Sea) as revealed by long-term pCO2 data. Oceanologia 57, 375–385. https://doi.org/10.1016/j.oceano.2015.07.001.
Seppälä, J., Ylöstalo, P., Kaitala, S., Hällfors, S., Raateoja, M., Maunula, P., 2007. Ship-of-opportunity based phycocyanin fluorescence monitoring of the filamentous cyanobacteria bloom dynamics in the Baltic Sea. Estuar. Coast. Shelf Sci. 73, 489–500. https://doi.org/10.1016/j.ecss.2007.02.015.
Seppälä, J., Maunula, P., Haavisto, N., Rehder, G., Karlson, B., Wranne, A.W., Lips, U., Kikas, V., Jaanus, A., London, L., Laakso, L., 2021. Transnational FerryBox monitoring in the Baltic Sea: Common measures for quality assurance. In: 2021 International Workshop on Metrology for the Sea; Learning to Measure Sea Health Parameters (MetroSea), pp. 121–125. https://doi.org/10.1109/MetroSea52177.2021.9611608.
Stal, L.J., Albertano, P., Bergman, B., von Bröckel, K., Gallon, J.R., Hayes, P.K., Sivonen, K., Walsby, A.E., 2003. BASIC: Baltic Sea cyanobacteria. An investigation of the structure and dynamics of water blooms of cyanobacteria in the Baltic Sea—responses to a changing environment. Cont. Shelf Res. 23, 1695–1714. https://doi.org/10.1016/j.csr.2003.06.001.
Suikkanen, S., Kaartokallio, H., Hällfors, S., Huttunen, M., Laamanen, M., 2010. Life cycle strategies of bloom-forming, filamentous cyanobacteria in the Baltic Sea. Deep-Sea Res. II Top. Stud. Oceanogr. 57, 199–209. https://doi.org/10.1016/j.dsr2.2009.09.014.
Thomas, H., Schneider, B., 1999. The seasonal cycle of carbon dioxide in Baltic Sea surface waters. J. Mar. Syst. 22, 53–67. https://doi.org/10.1016/S0924-7963(99)00030-5.
Vahtera, E., Conley, D.J., Gustafsson, B.G., Kuosa, H., Pitkänen, H., Savchuk, O.P., Tamminen, T., Viitasalo, M., Voss, M., Wasmund, N., Wulff, F., 2007. Internal ecosystem feedbacks enhance nitrogen-fixing cyanobacteria blooms and complicate management in the Baltic Sea. Ambio 36, 186–194. https://doi.org/10.1579/0044-7447(2007)36[186:iefenc]2.0.co;2.
Wanninkhof, R., 1992. Relationship between wind speed and gas exchange over the ocean. J. Geophys. Res. Oceans 97, 7373–7382. https://doi.org/10.1029/92JC00188.
Wanninkhof, R., 2014. Relationship between wind speed and gas exchange over the ocean revisited. Limnol. Oceanogr. Methods 12, 351–362. https://doi.org/10.4319/lom.2014.12.351.
Wasmund, N., 1997. Occurrence of cyanobacterial blooms in the Baltic Sea in relation to environmental conditions. Int. Rev. Hydrobiol. 82, 169–184. https://doi.org/10.1002/iroh.19970820205.
Wasmund, N., 2017. Recruitment of bloom-forming cyanobacteria from winter/spring populations in the Baltic Sea verified by a mesocosm approach. Boreal Environ. Res. 22, 445–455.
Wasmund, N., Siegel, H., 2008. Phytoplankton. In: State and Evolution of the Baltic Sea, 1952–2005. John Wiley & Sons, Ltd, pp. 441–481. https://doi.org/10.1002/9780470283134.ch15.
Wasmund, N., Voss, M., Lochte, K., 2001. Evidence of nitrogen fixation by non-heterocystous cyanobacteria in the Baltic Sea and re-calculation of a budget of nitrogen fixation. Mar. Ecol. Prog. Ser. 214, 1–14. https://doi.org/10.3354/meps214001.
Wasmund, N., Nausch, G., Schneider, B., Nagel, K., Voss, M., 2005. Comparison of nitrogen fixation rates determined with different methods: a study in the Baltic proper. Mar. Ecol. Prog. Ser. 297, 23–31. https://doi.org/10.3354/meps297023.
Weiss, R.F., 1970. The solubility of nitrogen, oxygen and argon in water and seawater. Deep-Sea Res. Oceanogr. Abstr. 17, 721–735. https://doi.org/10.1016/0011-7471(70)90037-9.
Weiss, R.F., 1974. Carbon dioxide in water and seawater: the solubility of a non-ideal gas. Mar. Chem. 2, 203–215. https://doi.org/10.1016/0304-4203(74)90015-2.
Weiss, R.F., Price, B.A., 1980. Nitrous oxide solubility in water and seawater. Mar. Chem. 8, 347–359. https://doi.org/10.1016/0304-4203(80)90024-9.
York, A., 2018. Marine biogeochemical cycles in a changing world. Nat. Rev. Microbiol. 16, 259. https://doi.org/10.1038/nrmicro.2018.40.
Zängl, G., Reinert, D., Rípodas, P., Baldauf, M., 2015. The ICON (ICOsahedral non-hydrostatic) modelling framework of DWD and MPI-M: description of the non-hydrostatic dynamical core. Q. J. R. Meteorol. Soc. 141, 563–579. https://doi.org/10.1002/qj.2378.